Available online at www.sciencedirect.com
SCIENCE DIRECT
Carbon 44 (2006) 2323–2329
CARBON
www.elsevier.com/locate/carbon

Band structure and absorption spectrum of double-walled zigzag carbon nanotubes in an electric field

G.W. Ho [a], Y.H. Ho [a], T.S. Li [b], C.P. Chang [c], M.F. Lin [a,*]

[a] Department of Physics, National Cheng Kung University, 1 Da-Suei Road, Tainan 70101, Taiwan, ROC
[b] Department of Electrical Engineering, Kun Shan University of Technology, Taiwan, ROC
[c] Center for General Education, Tainan Woman's College of Arts and Technology, Taiwan, ROC

Received 8 June 2005; accepted 11 February 2006
Available online 27 March 2006

Abstract

The electronic structure of the (9,0)–(18,0) double-walled zigzag carbon nanotubes in the presence of a uniform transverse electric field is studied by the tight-binding model. The electric field could induce the semiconductor–metal transition, change the direct gap into the indirect gap, alter the subband curvatures, destroy the double degeneracy, produce the new band-edge states, make more subbands group around the Fermi level, and widen the π-band width. Such effects are directly reflected in density of states and optical excitation spectra. The absorption spectra exhibit a lot of prominent peaks, mainly owing to the rich one-dimensional energy subbands. The intensity, the number, and the frequency of absorption peaks are strongly modulated by the electric field. The modulation of electronic and optical properties is amplified by the parallel magnetic field. The predicted electronic and optical properties can be, respectively, verified by the conductance measurements and the optical spectroscopy.

Keywords: Carbon nanotubes; Electronic structure; Optical properties

1. Introduction

Carbon nanotubes (CNTs) were first discovered by Iijima in 1991 [1]. Owing to their extraordinary electronic properties, CNTs have attracted much interest and are believed to be of great potential for the next generation nanoscale electronic devices [2–6]. A hollow cylinder made up of a single rolled-up graphite sheet is a single-walled carbon nanotube (SWCNT), and multi-walled carbon nanotubes (MWCNTs) are composed of several concentric hollow cylinders. Double-walled carbon nanotubes (DWCNTs) are the simplest MWCNTs, and they provide a good platform for studying the intertube interactions in MWCNTs. Besides, CNTs could be packed together to form a nanotube bundle as a result of Van der Waals interactions. Recently, it is feasible to synthesize highly purified SWCNTs [7] and DWCNTs [8] efficiently. Well-aligned SWCNTs and DWCNTs, respectively, can also be obtained to meet specific experimental needs [9,10].

The geometric structure of a SWCNT, which uniquely determines the band structure, can be characterized by the chiral indices (m,n) [11]. For example, $(m,0)$ represents a zigzag SWCNT, in which there are m zigzag cusps along the azimuthal direction. Carbon nanotubes can be classified as (I) metals for $m = n$, (II) narrow-gap semiconductors for $2m + n = 3I, m \neq n$ (I is an integer), and (III) moderate-gap semiconductors for $2m + n \neq 3I$ [12,13]. The important difference between type-I and type-II SWCNTs mainly comes from the curvature effect (the misorientations of $2p_z$ orbitals on the cylindrical surface). Such energy gaps have been verified by the scanning tunneling microscopy (STM) [14–16]. The transverse electric field $\mathbf{E}_\perp$ perpendicular to the nanotube axis ($\|\hat{z}$) will drastically change the band structure and may lead to the semiconductor–metal

* Corresponding author. Tel.: +886 627 575 7565272; fax: +886 627 47995.
E-mail address: mflin@mail.ncku.edu.tw (M.F. Lin).

0008-6223/$ - see front matter © 2006 Elsevier Ltd. All rights reserved.
doi:10.1016/j.carbon.2006.02.016

transition [17–19]. Moreover, energy bands are also strongly modulated by the magnetic field. The main effects of the magnetic field including Aharonov–Bohm effect and the destruction of state degeneracy are predicted and observed in carbon nanotubes [20,21]. Because external fields alter the band structure, they provide good tools to modulate the behavior of the nanotube and deserve a thorough study.

Apart from SWCNTs, DWCNTs also attracted much attention, and a lot of researches were done in last few years, e.g., growth [22–25], geometric structures [26–29], electronic structures [30–32], transport properties [33,34], phonon spectra [35,36], and optical excitations [30]. DWCNTs are mainly synthesized via the arc discharge method [22,23] and the chemical vapor deposition method [24,25]. Fullerene peapods can be transformed to DWCNTs by heating or UV irradiation [37,38]. Recently, highly purified DWCNTs (over 95%) are obtained by the chemical vapor deposition method [8]. Raman scattering [26], TEM observation [27], and X-ray diffraction [28] are often used to identify DWCNTs. They all indicate that the radius difference between inner and outer nanotubes is in the range from 3.4 Å to 4.0 Å. Theoretical studies showed that band structure and stability of DWCNTs are mainly determined by the symmetric configurations [29–31]. The optimized intertube spacing from theoretical calculations is in good agreement with experiments. Besides the methods mentioned before, it is suggested that the optical spectroscopy would be another powerful tool in identifying DWCNTs, because band structures of different combined nanotubes will reflect on their optical absorption spectra.

Here, we are interested in the response of DWCNTs to the external electric and magnetic fields. We focus on the (9,0)–(18,0) zigzag DWCNTs and use the tight-binding model to investigate band structure, density of states, and optical absorption spectra. The effects due to curvature and intertube interactions are also included in the calculations. This study shows that energy gap is enlarged by the intertube interactions. Electronic properties are drastically modulated by the transverse electric field $\mathbf{E}_\perp$, e.g., the changes in energy gap, subband spacings, energy width, band-edge states, subband curvatures, state degeneracy, and Fermi level. The field-induced effects are directly reflected in the optical absorption spectra, such as the intensity, the number, and the frequency of absorption peaks. The electric field splits energy subbands and thus enriches absorption peaks. The modulations of electronic and optical properties are enhanced by the parallel magnetic field. The predicted energy gap and density of states could be tested by the conductance measurements. The optical spectroscopy [39–42] could be utilized to verify the calculated absorption spectrum.

2. The tight-binding model and the optical spectral function

The (9,0)–(18,0) zigzag DWCNTs, as shown in Fig. 1, are chosen for a model study. The configuration of the inner nanotube is enlarged (the heavy curves), and then is projected onto the outer nanotube (the light curves). Carbon atoms in both inner and outer nanotubes exist in the perfect hexagonal bond network without topological defects. This system has both translation and rotation symmetries, with periods $r_z = 1.5b$ and 10°. $b = 1.42$ Å is the C–C bond length. The chosen intertube distance $a = 3.52$ Å is close to the experimental data [22–28].

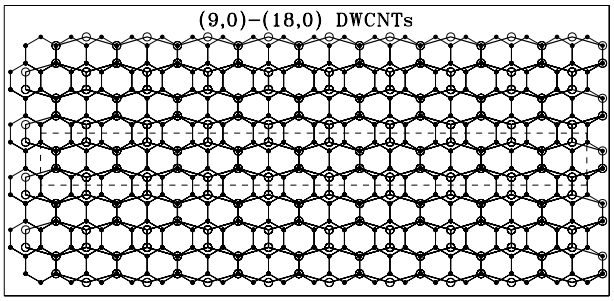

Fig. 1. The geometric structure of the coaxial (9,0)–(18,0) zigzag carbon nanotubes. The dashed rectangle encloses an enlarged unit cell.

The primitive cell of a SWCNT contains two carbon atoms, and the tight-binding Hamiltonian is a 2×2 Hermitian matrix. The DWCNTs have an enlarged primitive cell of 12 atoms, in which eight atoms and four atoms locate on the outer and inner nanotubes, respectively. The tight-binding Hamiltonian is a 12×12 Hermitian matrix. When DWCNTs exist in a uniform transverse electric field $\mathbf{E}_\perp$, a dipole-form perturbation potential $V = -eE_\perp y = -eE_\perp r\cos\theta$ should be added to each onsite energy. The electric field is chosen to be along the y-axis. θ is the azimuthal angle, and r is the nanotube radius. Also noted that charges on the nanotube surface would screen the transverse electric field [43]. That the static electric field used in the following calculations corresponds to the effective electric field might be relatively suitable. In order to describe this position-dependent perturbation, it is necessary to expand the unit cell to include all the atoms along the circumference (the dashed rectangle shown in Fig. 1). The tight-binding Hamiltonian becomes a 108×108 Hermitian matrix. The Hamiltonian of the DWCNTs can be divided into three parts [30]. The matrix element of $(H)_{36\times36}$ associated with the inner nanotube is expressed as

$$\langle\psi(\mathbf{R}_\mathrm{I})|H|\psi(\mathbf{R}'_\mathrm{I})\rangle = h_{rr}(\mathbf{R}_\mathrm{I},\mathbf{R}'_\mathrm{I})\mathrm{e}^{\mathrm{i}\mathbf{k}_\mathrm{I}\cdot(\mathbf{R}_\mathrm{I}-\mathbf{R}'_\mathrm{I})}. \tag{1a}$$

The matrix element of $(H)_{72\times72}$ related to the outer nanotube is

$$\langle\psi(\mathbf{R}_\mathrm{O})|H|\psi(\mathbf{R}'_\mathrm{O})\rangle = h_{rr}(\mathbf{R}_\mathrm{O},\mathbf{R}'_\mathrm{O})\mathrm{e}^{\mathrm{i}\mathbf{k}_\mathrm{O}\cdot(\mathbf{R}_\mathrm{O}-\mathbf{R}'_\mathrm{O})}. \tag{1b}$$

The matrix element of $(H)_{36\times72}$ from the intertube interactions is given by

$$\langle\psi(\mathbf{R}_\mathrm{I})|H|\psi(\mathbf{R}'_\mathrm{O})\rangle = W\cdot h_{rr}(\mathbf{R}_I,\mathbf{R}'_\mathrm{O})\mathrm{e}^{i(\mathbf{k}_I\cdot\mathbf{R}_\mathrm{I}-\mathbf{k}_\mathrm{O}\cdot\mathbf{R}'_\mathrm{O})}\cdot\mathrm{e}^{(a-d)/\delta}. \tag{1c}$$

$\mathbf{R}_\mathrm{I}$ and $\mathbf{R}_\mathrm{O}$ are, respectively, atomic positions on the inner and the outer nanotubes. The wave vector is

$\mathbf{k} = k_x\hat{x} + k_z\hat{z}$ ($k_x = 1/r$). The intratube hopping integral is $h_{rr}(\mathbf{R}_I, \mathbf{R}'_I) = V_{pp\pi}\cos\theta + 4(V_{pp\pi} - V_{pp\sigma})\sin^4(\theta/2)r^2/b^2$, where $V_{pp\pi} = \gamma_0 = -2.66$ eV and $V_{pp\sigma} = 6.38$ eV [30]. Similar results can be obtained for other intratube and intertube hopping integrals. As a result of the misorientations of $2p_z$ orbitals, the hopping integrals of $2p_z$ orbitals contain the π bonding $V_{pp\pi}$ and the σ bonding $V_{pp\sigma}$. For the intratube interactions, only the nearest neighbors are taken into account. The intertube atomic overlaps are neglected if the interatom distance on the projection plane is larger than $b = 1.42$ Å. The intertube interactions are assumed to decay exponentially with the interatom distance d, as shown in Eq. (1c). δ=0.45 Å and the parameter W in the intertube interactions is chosen to be 1/8 [44,45]. By diagonalizing the Hamiltonian matrix, state energy $E^h(J,k_z)$ and wave function $\psi^h(J,k_z)$ can be obtained. $h = v(c)$ corresponds to valence (conduction) subband. The longitudinal wave vector is confined within the first Brillouin zone $|k_z| \leqslant \pi/r_z$. Here J is only used to represent each subband, and it does not serve as a good quantum number. However, J in the absence of $\mathbf{E}_\perp$ means the angular momentum, as discussed in Ref. [30].

Density of states (DOS) directly reflects the main characteristics of energy subbands. It is associated with the number of optical excitation channels and useful in explaining the absorption spectra. DOS per unit length is defined as

$$D(\omega; E_\perp) = \sum_{h,J,\sigma}\int_{1stBZ}\frac{dk_z}{(2\pi)^2}\frac{\Gamma}{[\omega - E^h(J,k_z;E_\perp)]^2 + \Gamma^2}. \quad (2)$$

$\Gamma = 10^{-3}\ \gamma_0$ is the broadening parameter.

The optical absorption spectrum is determined by DOS and dipole matrix element and could be a simple but powerful tool in identifying CNTs. DWCNTs are assumed to exist in an electromagnetic field with electric polarization ($\mathbf{E}_\parallel$) parallel to the nanotube axis. When absorbing photons, electrons are excited from occupied states into unoccupied states. Since photons do not carry momentum, the initial and final states have the same longitudinal wave vector. That is to say, the optical selection rule is $\Delta k_z = 0$. For the vertical transitions, the optical spectral function calculated from the Fermi golden rule is

$$A(\omega; E_\perp) = \sum_{h,h'}\sum_{J,J'}\int_{1stBZ}\frac{dk_z}{2\pi} \cdot \left|\langle\psi^{h'}(J',k_z;E_\perp)\left|\frac{\hat{\mathbf{E}}_\parallel\cdot\mathbf{P}}{m_e}\right|\psi^h(J,k_z;E_\perp)\rangle\right|^2 \times \left[f(E^h(J,k_z;E_\perp)) - f(E^{h'}(J',k_z;E_\perp))\right] \times \left[\frac{\Gamma}{[\omega - \omega_{hh'}(J,k_z;E_\perp)]^2 + \Gamma^2}\right]. \quad (3)$$

$f(E^h(J,k_z;E_\perp))$ is the Fermi–Dirac distribution function. At $T = 0$, f equals to one (zero) for $E^h(J,k_z;E_\perp)$ smaller (larger) than the Fermi energy E_F. $\omega_{hh'}(J, k_z; E_\perp) = E^{h'}(J, k_z; E_\perp) - E^h(J, k_z; E_\perp)$ is the interband excitation energy. The optical transition rate is proportional to the square of the dipole matrix element, which is evaluated within the gradient approximation [46].

3. Electronic properties and optical spectra

Energy bands of the (9,0)–(18,0) zigzag DWCNTs are shown in Fig. 2(a)–(d). When the intertube interactions are neglected, occupied valence subbands (π) and unoccupied conduction subbands (π^*), as shown in Fig. 2(a), are symmetric about the Fermi level $E_F = 0$. All energy subbands have parabolic dispersions near the band edge, and they are doubly degenerated (neglect the spin degeneracy). The band-edge state for each subband is just located at $k_z^{ed} = 0$. There exists a small energy gap between the lowest conduction subband and the highest valence subband (denoted by J_ℓ), mainly owing to the curvature effect. Its magnitude is approximately given by $E_g = (3b^2/16r^2)\gamma_0$, e.g., $E_g = 22$ meV and 86.2 meV for the (18,0) and (9,0) CNTs, respectively.

The low-energy band structure is significantly affected by the intertube interactions (Fig. 2(b)). The band symmetry is destroyed and the Fermi level is shifted from zero to a finite value. That the strong hybridization of the $2p_z$ orbitals from the inner and the outer nanotubes is the main reason. The intertube interactions strongly modify the subband curvatures or the inverse effective masses of parabolic

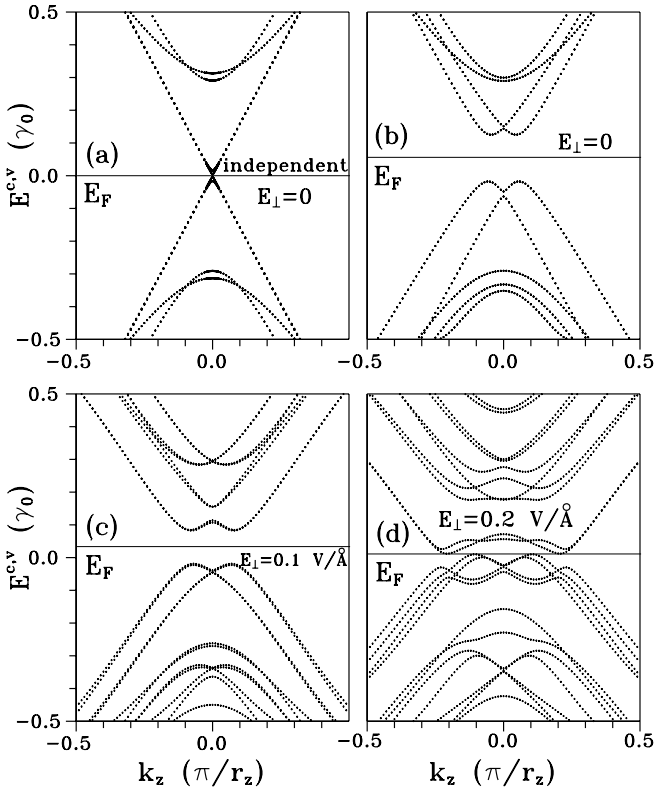

Fig. 2. The low-energy bands for (a) the independent case and $E_\perp = 0$, (b) $E_\perp = 0$, (c) $E_\perp = 0.1$ V/Å; (d) $E_\perp = 0.2$ V/Å.

energy subbands. They produce the new band-edge states of $k_z^{ed} \neq 0$ in the highest valence subband (the lowest conduction subband). Moreover, the intertube interactions drastically change the energy spacing between two band-edge states, and widen the energy gap. On the other hand, energy gap keeps a direct gap, and state degeneracy remains unchanged.

The electric field has a strong effect on electronic states, as shown in Fig. 2(c) and (d). There are more conduction subbands and valence subbands at low-energy or high-energy (not shown). The energy dispersions or the subband curvatures are drastically modulated by the electric field. Furthermore, there are more new band-edge states at $k_z^{ed} \neq 0$ in the $J \neq J_\ell$ subbands, or the band-edge states of the J_ℓ subbands exhibit large shifts. The electric field could destroy the double degeneracy and cause the subband crossing. When $\mathbf{E}_\perp$ is absent, there exist doubly degenerated subbands with angular momenta $\pm J$. The transverse electric field would make electrons on the cylindrical surfaces of DWCNTs encounter a dipole-form electric potential $V = -eEr(e^{i\theta} + e^{-i\theta})/2$. From the perturbation point of view, the new eigenstates could be obtained from the superposition of $|J\rangle$, $|J-1\rangle$, and $|J+1\rangle$. The coupling amplitudes are different for $|J-1\rangle$ and $|J+1\rangle$. The different effects of $\mathbf{E}_\perp$ on $|\pm J\rangle$ account for the destruction of the double degeneracy. The mixing effect among $|J\rangle$, $|J+1\rangle$, and $|J-1\rangle$ also leads to the energy lowering (enhancement) of the π^* (π) states, the produce of the new band-edge states, and the change of subband spacing. More energy bands approach to the Fermi level. Energy gap is gradually reduced by the increasing electric field, and it becomes a indirect gap at sufficiently large electric field (e.g., $E_\perp = 0.1$ V/Åin Fig. 2(c)). The semiconductor–metal transition occurs at the critical electric field $E_\perp^c = 0.2$ V/Å (Fig. 2(d)). When the electric field is higher than the critical field, energy gap is vanishing. In addition, the state degeneracy could also be destroyed by the magnetic field parallel to the nanotube axis [46]. $B_\parallel$ does not destroy the quantum number for each subband, but only causes the shift from J to $J + B_\parallel \pi r^2/\phi_0$ ($\phi_0 = hc/e$). The different shifts of $\pm J$ lead to the destruction of state degeneracy, and the shift of J causes the semiconductor–metal transition.

The dependence of low-energy states, energy gap, and energy width (E_w) on $\mathbf{E}_\perp$ deserves a closer investigation. The state energies of the $k_z = 0$ band-edge state, as shown in Fig. 3(a), strongly depend on the electric field. Subband spacings are clearly reduced or widened in the increasing of $E_\perp$. There exists a minimum energy spacing (E_{s0}) between occupied valence-band states and unoccupied conduction-band states. E_{s0} does not change from a finite value to zero during the variation of $E_\perp$. This subband spacing is not equal to energy gap, since the highest occupied state and the lowest unoccupied state do not correspond to the same k_z. The indirect energy gap, as shown in Fig. 3(b) by the dashed curve, would become vanishing at the critical electric field. Conduction subbands and valence subbands

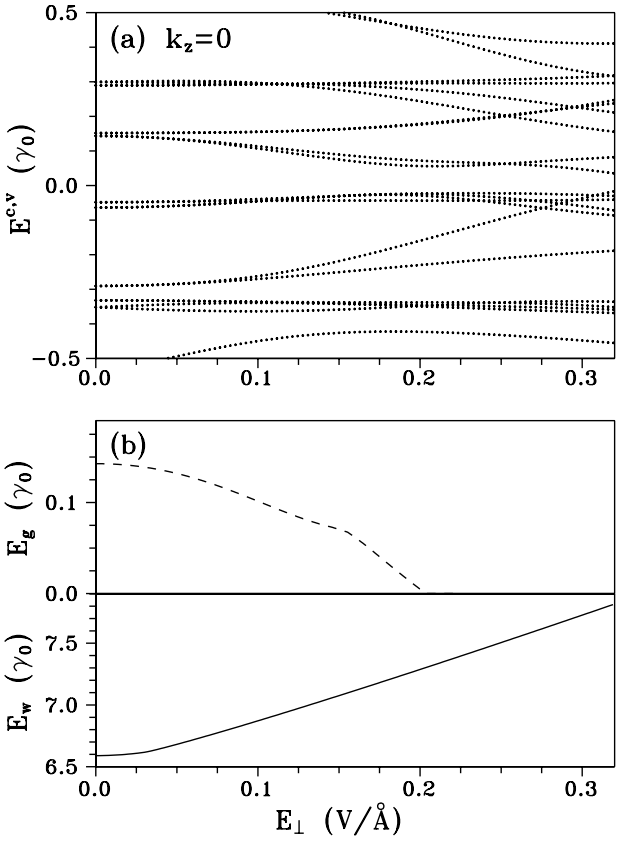

Fig. 3. The electric field-dependent (a) state energies of $k_z = 0$; (b) energy gap and energy width.

begin to overlap one another, when the electric field is larger than $E_\perp^c$. That is to say, DWCNTs are a gapless metal for $E_\perp \geqslant E_\perp^c$. In addition, energy subbands near the Fermi level keep parabolic even for the metallic case. The electric field also makes certain energy subbands extend into the low- (Fig. 3(a)) and high-energy regions simultaneously. Consequently, energy width grows with the increasing electric field, as shown in Fig. 3(b) by the solid curve.

The main characteristics of energy subbands, curvature, energy spacing, and state degeneracy, are directly reflected in density of states. DOS exhibits a lot of prominent peaks, as shown in Fig. 4(a)–(d). As a result of the 1D parabolic energy dispersions (Fig. 2(a)–(d)), such peaks are divergent in the asymmetric square-root form. Their positions are associated with the band-edge state energies, and their heights are proportional to the inverse square root of the subband curvature (or the square root of the effective mass). DOS is zero within the energy gap between two divergent peaks nearest to the Fermi level. Apparently, the number, the height, and the position of the divergent peaks are strongly affected by the intertube interactions (Fig. 4(b)) and the electric field (Fig. 4(c) and (d)). There are more pronounced peaks in the increasing of $E_\perp$, since the electric field could produce the new band-edge states and destroy the state degeneracy. The nonvanishing DOS at the critical field further illustrates that DWCNTs are metallic (Fig. 4(d)). The conductance measurements could

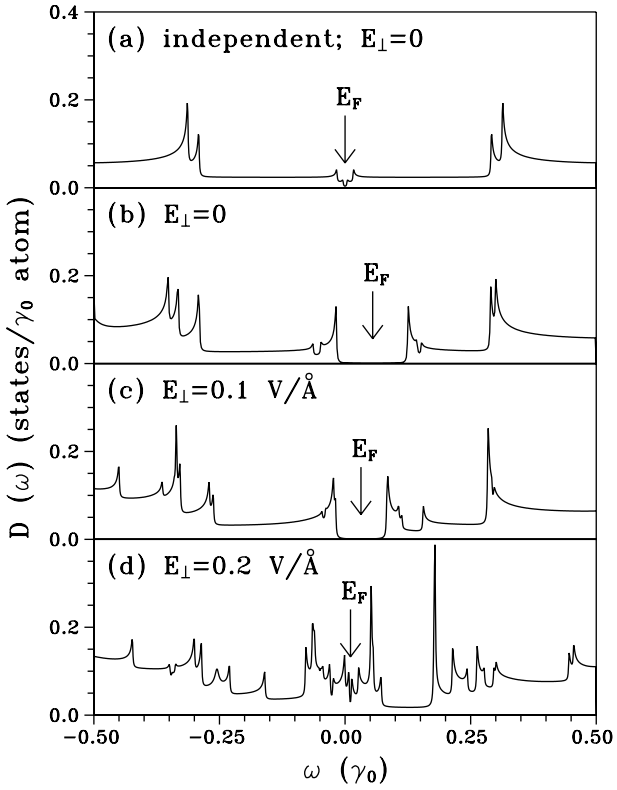

Fig. 4. The low-energy density of states for (a) the independent case and $E_\perp = 0$, (b) $E_\perp = 0$, (c) $E_\perp = 0.1$ V/Å; (d) $E_\perp = 0.2$ V/Å.

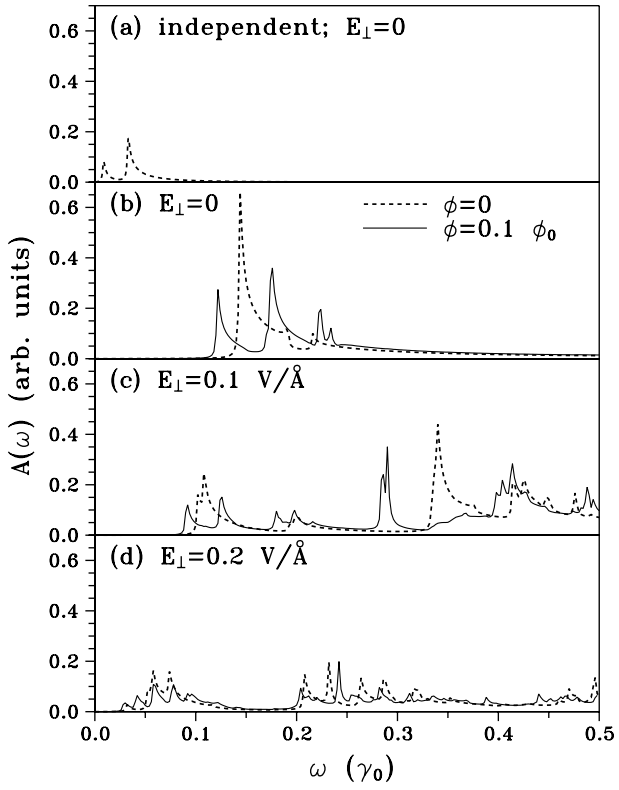

Fig. 5. The optical absorption spectra, with the electric polarization parallel to the nanotube axis, for (a) the independent case and $E_\perp = 0$, (b) $E_\perp = 0$, (c) $E_\perp = 0.1$ V/Å; (d) $E_\perp = 0.2$ V/Å. Also shown in (b)–(d) are those at $\phi = 0.1\ \phi_0$.

be used to examine the effects due to the electric field and the intertube interactions.

An electromagnetic field, with the longitudinal electric polarization, would make the occupied states exhibit the vertical transitions. DOS and dipole matrix element, respectively, determine the channel number and the strength of optical excitations. The low-frequency optical spectrum in the absence of the intertube interactions, as shown in Fig. 5(a), only exhibits two prominent absorption peaks. Such peaks have the asymmetric form of the inverse square root, as seen in DOS. They, respectively, come from the highest valence subbands of the inner and the outer nanotubes (Fig. 2(a)). The intertube interactions result in the shift of absorption frequency (ω_a), the change of spectrum intensity, and the increase of absorption peaks (Fig. 5(b)). At $\omega < 0.25\ \gamma_0$, there are three prominent absorption peaks. The two formers (the last one) come (results) from the two band-edge states of $k_z^{ed} = 0$ and $k_z^{ed} \neq 0$ in the highest valence subband (the band-edge state of $k_z^{ed} = 0$ in the next-highest valence subband) to those (that) of the lowest conduction subband (the next-lowest conduction subband) (Fig. 2(b)). The absorption frequency of the first peak is the threshold frequency. ω_{th} is equal to energy gap for a direct-gap system. But on the other hand, at $\omega > 0.25\gamma_0$, the pronounced absorption peaks are absent. The vertical optical excitations from the band-edge states in the highest and next-highest valence subbands (the lower valence subbands) to those of the higher conduction subbands (the lowest and next-lowest conduction subbands) do not exist. The vanishing dipole matrix elements only reflects the fact that the good quantum number, the angular momentum, in the absence of $E_\perp$ needs to be conserved ($\Delta J = 0$) [30]. Also noticed that such optical excitations survive at $E_\perp \neq 0$ (below), since the new eigenstates can be regarded as the superposition of the original $|J>$ and $|J \pm 1>$ states, as discussed earlier.

The number of absorption peaks is greatly enhanced by the increasing electric field, as shown in Fig. 5(c) and (d). The main reasons for this result are the destruction of state degeneracy, the new band-edge states, and the new optical excitations from lower valence subbands or higher conduction subbands (Fig. 2(c) and (d)). Each prominent peak corresponds to the vertical transition from the band-edge state of the valence subband to that of the conduction subband. However, it might also exist weak absorption peaks only due to a certain band-edge state in the valence subband or the conduction subband. For example, the first absorption peak at $E_\perp^c$, as shown in Fig. 5(d), is only associated with the highest band-edge state of the highest valence subband. At the sufficiently high electric field, the threshold frequency is independent of energy gap because of the indirect-gap characteristic, e.g., $\omega_{th} = 0.032\ \gamma_0$ at $E_\perp^c$.

The modulation of absorption spectrum by the electric field is strengthened by the parallel magnetic field, as shown in Fig. 5(b)–(d) by the solid curves. Under the suitable gauge $\mathbf{A} = \mathbf{B}_\parallel \times r/2 = Br\hat{\theta}/2$, electronic and optical

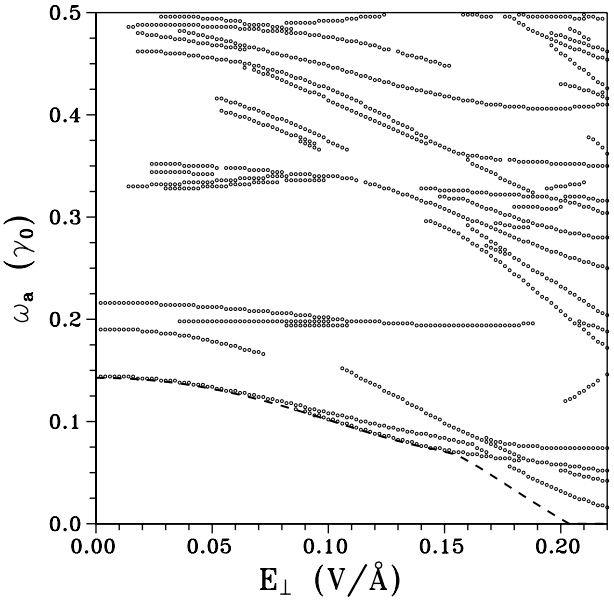

Fig. 6. The electric field-dependent absorption frequencies. Energy gap is also shown for comparison.

properties are obtained by adding the Peierls phase $G = \int \vec{\mathbf{A}} \cdot d\vec{r}$ in the Hamiltonian matrix elements. The parallel magnetic field can induce the different subband spacings, change the subband curvatures, and amplify the destruction of state degeneracy. However, $\mathbf{B}_\parallel$ does not produce the new band-edge states and alter the direct- or indirect-gap characteristic. The magneto-optical spectrum thus exhibits clearer absorption peaks, e.g., the larger frequency difference between two neighboring absorption peaks.

The strong dependence of the absorption frequencies on the electric field is shown in Fig. 6. Three absorption peaks exist at $E_\perp = 0$ and then the number of absorption peaks grows quickly in the increasing of $E_\perp$. There are a lot of absorption peaks even for small $E_\perp$. Most of absorption peaks survive at a certain electric field range. The absorption frequencies are reduced or enhanced by the increasing $E_\perp$. The threshold frequency, which is related to the highest band-edge state in the highest valence subband, decreases rapidly. It is close to energy gap for small $E_\perp$, while there is a clear difference between them for large $E_\perp$. The above-mentioned results clearly illustrate that electronic properties are dramatically changed by the electric field. The predicted absorption frequencies can be test by the optical spectroscopy [39–42].

4. Concluding remarks

In this work, electronic and optical properties of the (9,0)–(18,0) zigzag DWCNTs are studied. We use the tight-binding model to investigate band structure, density of states, and optical absorption spectra. The transverse electric field, the parallel magnetic field, the intertube interactions, and the curvature effect are included in the calculations. Energy dispersions, energy gap, subband spacings, energy width, state degeneracy, band-edge states, and Fermi level strongly depend on the electric field. $\mathbf{E}_\perp$ could lead to the semiconductor–metal transition, change the direct gap into the indirect gap, alter the subband curvatures, destroy the double degeneracy, produce the new band-edge states, make more subbands group around the Fermi level, and widen the π-band width. The predicted electronic properties could be examined by the conductance measurements. The effects due to the electric field are also reflected in optical excitation spectra. There are a lot of prominent absorption peaks, mainly owing to the rich one-dimensional energy subbands. The intensity, the number, and the frequency of abosorption peaks are strongly modulated by the electric field. As a result of the indirect-gap characteristic, the threshold absorption frequency does not correspond to the energy gap at sufficiently large electric field. The optical spetroscopy could be utilized to veirfy the calculated results. The modulations of electronic and optical properties are amplified by the parallel magnetic field.

Finally, we make comments on the effects due to the curvature effects. In general, the curvature effects include the misorientations of pπ orbitals and the hybridization of pπ orbitals and $sp^2\sigma$ orbitals. The former is included in the intratube and the intertube hopping integrals (Eq. (1)). The intratube hopping integrals, with the misorientation of $p\pi$ orbitals, are important for type-II SWCNTs. For example, $(3m,0)$ zigzag CNTs are narrow-gap semiconductors. The calculated energy gaps are well fitted by $(3b^2/16r^2)\gamma_0$, which are almost identical to those obtained by the $p\pi$-electronic tight-binding model [13]. The predicted narrow-gaps have been verified by the STM measurements on $(3m,0)$ zigzag SWCNTs ((9,0),(12,0);(15,0) CNs) [16]. The consistence between theory and experiment suggests that the $\pi - \sigma$ hybridization is not strong for CNTs with radii larger than that of the (9,0) CNT. On the other hand, the hybridization of $p\pi$ orbitals and $sp^2\sigma$ orbitals makes SWCNTs with radii smaller than that of the (6,0) CNT exhibit the metallic behavior [47]. Moreover, it dominates over the metallization of the (7,0)–$(m,0)$ DWCNTs ($m = 16,17,19;20$) [31]. These results show that the hybridization of $p\pi$ orbitals and $sp^2\sigma$ orbitals is strong for DWCNTs with inner nanotubes smaller than that of the (7,0) CNT. The π–σ hybridization quickly declines in the increasing of the nanotube radius. It exists in (9,0)–(18,0) DWCNTs. However, whether it plays an important role on the low-energy electronic properties needs to make a further study.

Acknowledgement

This work was supported in part by the National Sience Cuncil of Taiwan under Grant Nos. NSC 93-2112-M-006-002, NSC 93-2112-M-145-001; NSC 93-2112-M-165-001.

References

[1] Iijima S. Helical microtubules of graphitic carbon. Nature 1991; 354(6348):56–8.

[2] Dekker C. Carbon nanotubes as molecular quantum wires. Phys Today 1999;52:22–8.
[3] Tans SJ, Verschueren RM, Dekker C. Room-temperature transistor based on a single carbon nanotube. Nature 1998;393(6680):49–52.
[4] Tans SJ, Devoret MH, Dai H, Thess A, Smalley RE, Geerligs LJ, et al. Individual single-wall carbon nanotubes as quantum wires. Nature 1997;386(6624):474–7.
[5] Natori K, Kimura Y, Shimizu T. Characteristics of a carbon nanotube field-effect transistor analyzed as a ballistic nanowire field-effect transistor. J Appl Phys 2005;97(3):034306(7).
[6] Hoenlein W, Kreupl F, Duesberg GS, Graham AP, Liebau M, Seidel RV, et al. Carbon nanotube applications in microelectronics. IEEE Trans Components Packag Technol 2004;27(4):629–34.
[7] Hata K, Futaba DN, Mizuno K, Namai T, Yumura M, Iijima S. Water-assisted highly efficient synthesis of impurity-free single-walled carbon nanotubes. Science 2004;306(5700):1362–4.
[8] Endo M, Muramatsu H, Hayashi T, Kim YA, Terrones M, Dresselhaus MS. 'Buckypaper' from coaxial nanotubes. Nature 2005;433(7025):476.
[9] Li ZM, Tang ZK, Liu HJ, Wang N, Chan CT, Saito R, et al. Polarized absorption spectra of single-walled 4 Å carbon nanotubes aligned in channels of an $AlPO_4$-5 single crystal. Phys Rev Lett 2001;87(12):127401(4).
[10] Ren W, Li F, Cheng HM. Polarized Raman analysis of aligned double-walled carbon nanotubes. Phys Rev B 2005;71(11):115428(5).
[11] Lin MF, Shung KWK. Magnetoconductance of carbon nanotubes. Phys Rev B 1995;51(12):7592(6).
[12] Hamada N, Sawada S, Oshiyama A. New one-dimensional conductors: graphitic microtubules. Phys Rev Lett 1992;68(10):1579–81.
[13] Kane CL, Mele EJ. Size, shape, and low-energy electronic structures of carbon nanotubes. Phys Rev Lett 1997;78(10):1932–5.
[14] Wildoer JWG, Venema LC, Rinzler AG, Smalley RE, Dekker C. Electronic structure of atomically resolved carbon nanotubes. Nature 1998;391(6662):59–62.
[15] Odom TW, Huang JL, Kim P, Lieber CM. Atomic structure and electronic properties of single-walled carbon nanotubes. Nature 1998;391(6662):62–4.
[16] Ouyang M, Huang JL, Cheung CL, Lieber CM. Energy gaps in "metallic" single-walled carbon nanotubes. Science 2001;292(5517):702–5.
[17] Kim YH, Chang KJ. Subband mixing rules in circumferentially perturbed carbon nanotubes: effects of transverse electric fields. Phys Rev B 2001;64(15):153404(4).
[18] Zhou X, Chen H, Zhong-can OY. Can electric field-induced energy gaps in metallic carbon nanotubes? J Phys Condens Matter 2001;13(27):L635–40.
[19] O'Keeffe J, Wei C, Cho K. Band structure modulation for carbon nanotubes in a uniform electric field. Appl Phys Lett 2002;80(4):676–8.
[20] Roche S, Dresselhaus G, Dresselhaus MS, Saito R. Aharonov–Bohm spectral features and coherence lengths in carbon nanotubes. Phys Rev B 2000;62(23):16092–9.
[21] Zaric S, Ostojic GN, Kono J, Shaver J, Moore VC, Strano MS, Hauge RH, Smalley RE, Wei X. Optical signatures of the Aharonov–Bohm phase in single-walled carbon nanotubes. Science 2004;304(5674):1129–31.
[22] Hutchison JL, Kiselev NA, Krinichnaya EP, Krestinin AV, Loutfy RO, Morawsky AP, et al. Double-walled carbon nanotubes fabricated by a hydrogen arc discharge method. Carbon 2001;39(5):761–70.
[23] Li L, Li F, Liu C, Cheng HM. Synthesis and characterization of double-walled carbon nanotubes from multi-walled carbon nanotubes by hydrogen-arc discharge. Carbon 2005;43(3):623–9.
[24] Ren W, Li F, Chen J, Bai S, Cheng HM. Morphology, diameter distribution and Raman scattering measurements of double-walled carbon nanotubes synthesized by catalytic decomposition of methane. Chem Phys Lett 2002;359(3–4):196–202.
[25] Zhu J, Yudasaka M, Iijima S. A catalytic chemical vapor deposition synthesis of double-walled carbon nanotubes over metal catalysts supported on a mesoporous material. Chem Phys Lett 2003;380(5–6):496–502.
[26] Li F, Chou SG, Ren W, Gardecki JA, Swan AK, Unlu MS, et al. Identification of the constituents of double-walled carbon nanotubes using Raman spectra taken with different laser-excitation energies. J Mater Res 2003;18(5):1251–8.
[27] Hashimoto A, Suenaga K, Urita K, Shimada T, Sugai T, Bandow S, et al. Atomic correlation between adjacent graphene layers in double-wall carbon nanotubes. Phys Rev Lett 2005;94(4):045504(4).
[28] Zuo JM, Vartanyants I, Gao M, Zhang R, Nagahara LA. Atomic resolution imaging of a carbon nanotube from diffraction intensities. Science 2003;300(5624):1419–21.
[29] Charlier JC, Michenaud JP. Energetics of multilayered carbon tubules. Phys Rev Lett 1993;70(12):1858–61.
[30] Ho YH, Chang CP, Shyu FL, Chen SC, Lin MF. Electronic and optical properties of double-walled armchair carbon nanotubes. Carbon 2004;42(15):3159–67.
[31] Okada S, Oshiyama A. Curvature-induced metallization of double-walled semiconducting zigzag carbon canotubes. Phys Rev Lett 2003;91(21):216801(4).
[32] Choi HC, Kim SY, Jang WS, Bae SY, Park J, Kim KL, et al. X-ray photoelectron spectroscopy studies of double-walled carbon nanotube bundles synthesized using thermal chemical vapor deposition. Chem Phys Lett 2004;399(1–3):255–9.
[33] Uryu S. Electronic states and quantum transport in double-wall carbon nanotubes. Phys Rev B 2004;69(7):075402(10).
[34] Kajiura H, Huang H, Bezryadin A. Quasi-ballistic electron transport in double-wall carbon nanotubes. Chem Phys Lett 2004;398(4–6):476–9.
[35] Bandow S, Chen G, Sumanasekera GU, Gupta R, Yudasaka M, Iijima S, et al. Diameter-selective resonant Raman scattering in double-wall carbon nanotubes. Phys Rev B 2002;66(7):075416(8).
[36] Xia M, Zhang S, Zhang E, Zhao S, Zuo X. Vibrational spectra of double-wall carbon nanotubes. Phys Rev B 2004;69(23):233407(3).
[37] Bandow S, Takizawa M, Hirahara K, Yudasaka M, Iijima S. Raman scattering study of double-wall carbon nanotubes derived from the chains of fullerenes in single-wall carbon nanotubes. Chem Phys Lett 2001;337(1–3):48–54.
[38] Kalbac M, Kavan L, Juha L, Civis S, Zukalova M, Bittner M, et al. Transformation of fullerene peapods to double-walled carbon nanotubes induced by UV radiation. Carbon 2005;43(8):1610–6.
[39] Ugawa A, Rinzler AG, Tanner DB. Far-infrared gaps in single-wall carbon nanotubes. Phys Rev B 1999;60(16):11305(4).
[40] Kouklin N, Tzolov M, Straus D, Yin A, Xu JM. Infrared absorption properties of carbon nanotubes synthesized by chemical vapor deposition. Appl Phys Lett 2004;85(19):4463–5.
[41] Kazaoui S, Minami N, Yamawaki H, Aoki K, Kataura H, Achiba Y. Pressure dependence of the optical absorption spectra of single-walled carbon nanotube films. Phys Rev B 2000;62(3):1643–6.
[42] Kataura H, Kumazawa Y, Maniwa Y, Umezu I, Suzuki S, Ohtsuka Y, et al. Optical properties of single-walled carbon nanotubes. Synth Met 1999;103(1–3):2555–8.
[43] Ajiki H, Ando T. Aharonov–Bohm effect in carbon nanotubes. Physica B 1994;201:349–52.
[44] Ahn KH, Kim YH, Wiersig J, Chang KJ. Spectral correlation in incommensurate multiwalled carbon nanotubes. Phys Rev Lett 2003;90(2):026601(4).
[45] Roche S, Triozon F, Rubio A, Mayou D. Conduction mechanisms and magnetotransport in multiwalled carbon nanotubes. Phys Rev B 2001;64(12):121401(4).
[46] Shyu FL, Chang CP, Chen RB, Chiu CW, Lin MF. Magnetoelectronic and optical properties of carbon nanotubes. Phys Rev B 2003;67(4):045405(9).
[47] Blase X, Benedict LX, SHirley EL, Louie SG. Hybridyization effects and metallicity in small radius carbon nanotubes. Phys Rev Lett 1994;72(12):1878–81.